

Giant-tunable bidirectional Goos-Hänchen shifts via phase change material-based metasurfaces with quasi-bound states in continuum

Jiaqing Liu(刘佳晴), Yue Zheng(郑悦), Xiao Li(李潇), Jingwen Li(李静文), Guohao Zhang(张国昊), Daxing Dong(董大兴), Dongmei Liu(刘冬梅), Yuwen Jia(贾玉雯), Yangyang Fu(伏洋洋), and Youwen Liu(刘友文)
Citation: Chin. Phys. B, 2025, 34 (**7**): 074208. DOI: 10.1088/1674-1056/adcdee
http://cpb.iphy.ac.cn; http://iopscience.iop.org/cpb

What follows is a list of articles you may be interested in

High-efficiency Yb^{3+}-doped fiber laser with highly optical nonlinear Bi_4Br_4-based saturable absorber

Mengyuan Liu(刘梦媛), Yechao Han(韩烨超), Qi Liu(刘齐), Hao Teng(滕浩), Xiwei Huang(黄玺玮), Xiaowei Xing(邢笑伟), Xiangyu Qiao(乔向宇), Guojing Hu(胡国静), Xiao Lin(林晓), Haitao Yang(杨海涛), Zhiyi Wei(魏志义), and Wenjun Liu(刘文军)
Chin. Phys. B, 2025, 34 (**6**): 064202. DOI: 10.1088/1674-1056/adc664

Enhancing the Goos-Hänchen shift based on quasi-bound states in the continuum through material asymmetric dielectric compound gratings

Xiaowei Jiang(江孝伟), Bin Fang(方彬), and Chunlian Zhan(占春连)
Chin. Phys. B, 2024, 33 (**3**): 034206. DOI: 10.1088/1674-1056/acf661

Active control of surface plasmon polaritons with phase change materials

Yuan-Zhen Qi(漆元臻), Qiao Jiang(蒋瞧), Hong Xiang(向红), and De-Zhuan Han(韩德专)
Chin. Phys. B, 2023, 32 (**10**): 104202. DOI: 10.1088/1674-1056/accd5a

Antimonene-based saturable absorber for a soliton mode-locked and *Q*-switched fiber laser in the 2 μm wavelength region

H Ahmad, B Nizamani, M Z Samion, N Yusoff, and M F Ismail
Chin. Phys. B, 2023, 32 (**6**): 064205. DOI: 10.1088/1674-1056/ac891f

Polarization readout analysis for multilevel phase change recording by crystallization degree modulation

Lin Jin-Cheng (林金成), Long Guo-Yun (龙国云), Wang Yang (王阳), Wu Yi-Qun (吴谊群)
Chin. Phys. B, 2013, 22 (**12**): 124208. DOI: 10.1088/1674-1056/22/12/124208

Giant-tunable bidirectional Goos–Hänchen shifts via phase change material-based metasurfaces with quasi-bound states in continuum

Jiaqing Liu(刘佳晴)[1], Yue Zheng(郑悦)[1], Xiao Li(李潇)[2,3], Jingwen Li(李静文)[2,3], Guohao Zhang(张国昊)[2,3], Daxing Dong(董大兴)[2,3], Dongmei Liu(刘冬梅)[1], Yuwen Jia(贾玉雯)[1], Yangyang Fu(伏洋洋)[2,3,†], and Youwen Liu(刘友文)[2,3,‡]

[1] *College of Science, North China University of Science and Technology, Tangshan* 063210, *China*
[2] *College of Physics, Nanjing University of Aeronautics and Astronautics, Nanjing* 211106, *China*
[3] *Key Laboratory of Aerospace Information Materials and Physics (NUAA), MIIT, Nanjing* 211106, *China*

(Received 17 February 2025; revised manuscript received 12 April 2025; accepted manuscript online 17 April 2025)

We propose a novel approach for investigating the tunable Goos–Hänchen (GH) shift via an all-dielectric metasurface that incorporates phase change materials (PCMs). By introducing material asymmetry through the reconfigurable characteristic of PCMs while maintaining fixed geometric parameters, we can achieve tunable dual quasi-bound states in the continuum with ultrahigh quality factors (Q factors). Enabled by such tunable dual modes with significant phase changes, the PCM-based metasurface exhibits giant-tunable bidirectional GH shifts compared to conventional metasurfaces. Notably, the GH shift exhibits multidimensional tunability, including PCM-driven switching (amorphous to crystalline), incident-angle dependence (θ), and wavelength selectivity (λ). The maximum observed shift reaches approximately 10^4 wavelengths, accompanied by a corresponding Q factor of 10^7. Our work demonstrates its potential for applications in ultrahigh-precision multifunctional devices, from biosensing to reconfigurable nanophotonic switches.

Keywords: phase change materials, Goos–Hänchen shift, quasi-bound states in the continuum, tunable metasurfaces

PACS: 42.70.–a, 42.79.Dj, 78.20.Ci, 78.67.Pt

DOI: 10.1088/1674-1056/adcdee **CSTR:** 32038.14.CPB.adcdee

1. Introduction

Goos–Hänchen (GH) shift, discovered at the interface between two media, involves a tiny deviation from the position predicted by geometric optics when the incident beam is totally reflected.[1] According to the direction of Poynting energy, it can be categorized into positive (forward direction) and negative shifts (backward direction).[2] Positive GH shift allows for the separation of the incident and reflected beams and is beneficial for applications such as sensors and switches,[3–5] while the negative shift forms a closed optical path and can be used for optical storage.[6–8] However, the values of the two initial GH shifts are both comparable to the operating wavelength, resulting in an urgent need for enhancement. Currently, conventional methods to enhance the GH shift involve exploiting the Brewster effect[9,10] and transmission-type resonance,[11] where the reflection phase undergoes distinct variations around the resonance angle, leading to significant relative shifts.[12] However, despite the advancements in various methods for enhancement, a significant challenge in detection arises due to their location at reflection dips. Furthermore, these methods are restricted by their unidirectional enhancement characteristics, which impose limitations on their applications. To overcome these limitations, several approaches based on novel materials have been proposed, such as left-handed slabs,[13,14] photonic crystals,[15,16] two-dimensional materials,[17–20] and epsilon-near-zero metamaterials.[21,22] Additionally, quasi-bound states in the continuum (quasi-BICs) have been recently suggested as solutions, since they can provide ultrahigh quality factors (Q factor) resonance with dramatic phase changes, leading to total reflection of the incident beam and enabling the realization of giant GH shifts.[23–26]

The quasi-BIC, arising from the corresponding bound state in the continuum (BIC) with an infinite Q factor, can be generated by breaking various symmetries in periodic metasurfaces. However, since one asymmetry corresponds to a single quasi-BIC, only unidirectional enhancement of GH shift can be achieved.[23] To enable multifunctionality in compact structures, recent research has focused on dual quasi-BICs which can enhance both positive and negative GH shifts.[24] Over the past few years, researchers have explored different methods to obtain dual quasi-BICs,[27–29] such as period en-

†Corresponding author. E-mail: yyfu@nuaa.edu.cn
‡Corresponding author. E-mail: ywliu@nuaa.edu.cn

© 2025 Chinese Physical Society and IOP Publishing Ltd. All rights, including for text and data mining, AI training, and similar technologies, are reserved.

gineering, width modulation, and oblique incidence. Though these approaches exhibit capabilities in enhancing GH shifts, most of them depend on traditional materials that require expensive and inconvenient structural modifications to attain multifunctionality. Based on phase-change materials, Jiang[30] and some others realized a tunable negative GH shift by material asymmetric metagratings, but they are still limited by the bidirectional enhancement. Therefore, it remains challenging to achieve giant and tunable GH shifts in both positive and negative directions without structural reconstruction.

Recently, we found that the dual quasi-BICs can be achieved by breaking the geometric and material symmetries simultaneously in the phase-change material (PCM)-based metasurface under normal incidence.[31] Moreover, such dual quasi-BIC modes can also be obtained by breaking either of the two symmetries under oblique incidence. Multiple degrees of freedom to obtain dual quasi-BIC modes show the tunability to achieve two different GH shifts (positive and negative). Since the structure cannot be changed once fabricated, the material asymmetry should be adopted at oblique incidence conditions to obtain dual quasi-BIC modes in a fixed structure, which can be realized by introducing a proper PCM. By flexibly modulating the permittivity of a PCM at oblique incidence via external stimuli, selective excitation of forward- and backward-propagating resonant guided modes can be obtained. Thus, the Q factor of the quasi-BIC mode is adjustable, leading to giant-tunable bidirectional GH shifts. Assisted by the dual quasi-BICs and adjustable permittivity of PCM, our proposed metasurface exhibits giant-tunable bidirectional GH shifts, and further undergoes modulation across multiple dimensions, including fixed wavelengths (at various incident angles) or fixed incident angles (at different wavelengths).

2. Structure and numerical optimization

Figure 1(a) presents a schematic diagram of the proposed metasurface consisting of grating, waveguide, and substrate layers with a period of p. To construct an all-dielectric metasurface, lossless materials are chosen for all the layers at the operating wavelength (1550 nm). Antimony selenide Sb_2Se_3 is selected as the PCM for grating I due to the characteristic of no loss ($k = 0$). By operating the reversible phase transition between amorphous (A) and crystalline (C) states, the permittivity of Sb_2Se_3 is changed from $\varepsilon_{g1}^{A} = (3.285 + 0\mathrm{i})^2$ to $\varepsilon_{g1}^{C} = (4.050 + 0\mathrm{i})^2$, and the values are almost unchangeable in the near-infrared range.[32,33] To achieve a practical tunable range of material asymmetry, grating II is fixed as silicon (Si, $\varepsilon_{g2} = 3.48^2$), whose permittivity falls between that of ε_{g1}^{A} and ε_{g1}^{C}. The material asymmetry is related to the variable permittivity of Sb_2Se_3, i.e., which is defined by $\beta = \varepsilon_{g1} - \varepsilon_{g2}$ ($\beta \in [-0.109, 0.354]$). The widths of the two gratings are denoted by w, the space between them is s and the duty ratios are $f_g = w/p$, $f_0 = s/p$. Additionally, silicon carbide (SiC, $\varepsilon_s = 2.56^2$) is selected as the substrate and gallium arsenide (GaAs, $\varepsilon_{wg} = 3.38^2$) is chosen as the waveguide layer.

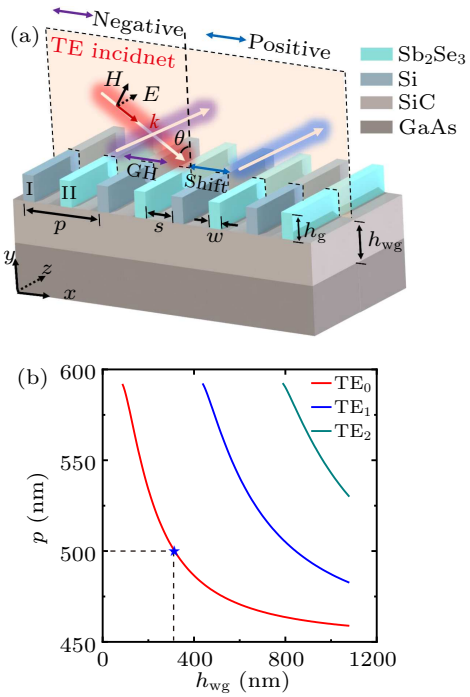


Fig. 1. (a) Schematics diagram of the PCM-based metasurface with positive and negative GH shifts, consisting of substrate, waveguide, and grating layers. (b) Dispersion relationship of the guided mode resonance under oblique incidence at 1550 nm, including TE_0 (red), TE_1 (blue), and TE_2 (green) modes. The selected parameters $(p, h_{wg}) = (500, 313)$ nm for TE_0 mode are denoted by the blue star.

In our proposed structure, dual quasi-BICs originate from the guided mode resonance (GMR), which is essentially the coupling between the guided mode in the waveguide layer (β_{wg}) and the incident tangential wave vector in the air ($k_0 \sin\theta$) via an additional wave vector from the grating layer. The GMR condition can be expressed as

$$k_x^n = k_0 \sin\theta - G_g^n = \beta_{wg}, \tag{1}$$

in which k_0 is the wave vector in air, θ is the incident angle, and $G_g^n = 2n\pi/p$ is the n-th order reciprocal lattice vector of the grating layer. Here we consider $n = \pm 1$ for the diffraction order of the grating layer. For an incident transverse electric (TE) wave, the dispersion relationship of the fundamental TE_0 mode is satisfied as

$$\sigma_{wg} h_{wg} = \arctan\frac{\sigma_g}{\sigma_{wg}} + \arctan\frac{\sigma_s}{\sigma_{wg}}, \tag{2}$$

where $\sigma_{wg} = (k_0^2\varepsilon_{wg} - \beta_{wg}^2)^{1/2}$, $\sigma_g = (\beta_{wg}^2 - k_0^2\varepsilon_g)^{1/2}$, $\sigma_s = (\beta_{wg}^2 - k_0^2\varepsilon_s)^{1/2}$, and ε_g represents the permittivity of the grating layer, i.e., $\varepsilon_g = f_g(\varepsilon_{g1} + \varepsilon_{g2}) + (1 - 2f_g)\varepsilon_0$ ($\varepsilon_0 = 1$ is the permittivity of air). In the case of oblique incidence $\theta = 3^\circ$ and $w = 60$ nm for a fixed symmetric metasurface, the relationship between p and h_{wg} can be calculated by Eq. (2) (see Fig. 1(b)). Solutions of the TE_0 mode are chosen as $(p, h_{wg}) = (500, 313)$ nm for a relatively thin thickness of

the entire subwavelength structure (denoted by the blue star). Since the height of gratings h_g has little impact on the reflection spectrum, here we take the value as 220 nm for an example. Then the corresponding reflectivity simulated by COMSOL is shown in Fig. 2(a) for a suitable range, i.e., $\beta \in [0.36, 0.36]$, which includes the maximum material asymmetry to enable the demonstration of the symmetry-broken BICs in subsequent sections. According to the reflection characteristic of the relevant mode, the GH shift can be calculated by

$$S_{GH} = -(\lambda/2\pi)\cdot(\partial\varphi/\partial\theta), \tag{3}$$

where $\partial\varphi/\partial\theta$ represents the phase change corresponding to the incident angle. The phase change exhibits a proportionality to the Q factor of the mode (peak). However, when $\beta = 0$ and $\theta = 3°$, no reflection peak is present and the value of the Q factor cannot be obtained. To further optimize a higher Q factor for the investigated modes, the Q factor of the distinct reflection peaks are accurately calculated by $Q = f_r/2f_i$, in which f_r/f_i is the real/imaginary part of the eigenfrequency simulated by COMSOL. Here, the reflection spectrum of $\beta = 0.1$ is exhibited as an illustrative example to show the two sharp reflection peaks (see Fig. 2(b)). The peak with higher frequency corresponds to the even mode, and the lower peak represents the odd one, with parity defined by the symmetric axis (black dashed line) of the supercell revealed in Figs. 2(c) and 2(f). The frequency of the odd mode peak is approximately 192.892 THz (1554 nm), while the other is around 199.372 THz (1504 nm). The corresponding eigenfrequencies of both modes are $192.877 + 0.0034968\mathrm{i}$ THz (odd, $Q \sim 2.76 \times 10^4$) and $199.298 + 0.0016363\mathrm{i}$ THz (even, $Q \sim 6.09 \times 10^4$). Since the corresponding eigenwavelengths cover two continuous band ranges under different crystallization rates (*CR*s), and different resonance peaks exhibit distinct Q factors, the incident wavelength has also emerged as a significant factor in modulating the GH shift within a certain wavelength range. Furthermore, according to the nonzero imaginary parts of eigenfrequencies and leaked electric fields in Fig. S1 of supplementary materials, these two different modes are both confirmed to be quasi-BICs.

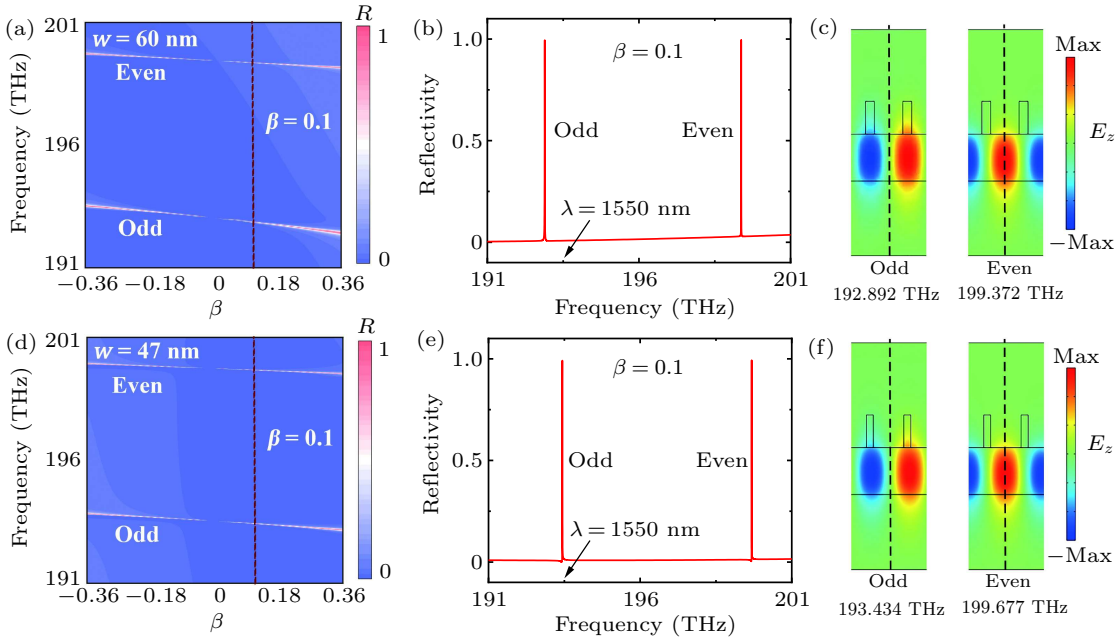


Fig. 2. Numerical reflection spectra of the metasurface at the oblique incidence of $\theta = 3°$, (a) within the range of $\beta \in [-0.36, 0.36]$, (b) the red dash line in panel (a) ($\beta = 0.1$), and panel (c) z components of the electric fields associated with two peaks in panel (b). Panels (a)–(c) are the results when $w = 60$ nm. Panels (d)–(f) are the corresponding results of panels (a)–(c) when $w = 47$ nm, respectively. The lower frequency represents the odd mode, while the higher one denotes the even mode.

However, it is observed that a discrepancy exists between the central frequency of the odd mode and our operating wavelength (see Fig. 2(b)). This deviation arises due to the higher-order Fourier expansion of the equivalent permittivity of the inhomogeneous grating layer (ε_g') in solving Eq. (2), which becomes imperative because of the introduced material asymmetry.[29] But the presence of an imaginary component in ε_g' complicates the direct resolution of Eq. (2), then an approximate value ($\varepsilon_g' = \varepsilon_g$) is employed for the solution, resulting in the inaccuracies in the solutions of Eq. (2). Therefore, the parameters should be reoptimized. Since ε_g can be modulated by the width of gratings w (related to f_g), the optimal structural parameters (p, h_{wg}, w', h_g) are defined as (500, 313, 47, 220) nm. The corresponding optimized reflection spectra are presented in Figs. 2(d) and 2(e), where the peaks appear at around 1550 nm (odd, 193.434 THz) and 1501 nm (even, 199.677 THz), respectively. The corresponding eigenfrequencies are $193.425 + 0.0017619\mathrm{i}$ THz (odd, $Q \sim 5.49 \times 10^4$) and $199.595 + 0.0010135\mathrm{i}$ THz (even, $Q \sim 9.85 \times 10^4$), of which the imaginary parts are smaller than those mentioned before

optimization, indicating higher Q factors and larger GH shifts. Additionally, all the results simulated by COMSOL are consistent with the calculations obtained by the rigorous coupled wave analysis (RCWA), which are shown in Fig. S2 of supplementary materials.

3. Simulation and results

Since the selected Sb_2Se_3 exhibits diverse optical properties in amorphous ($\beta = -0.109$) and crystalline states ($\beta = 0.354$) when subjected to external stimuli, the corresponding reflection spectra with optimal parameters of the structure in such two states are shown in Figs. 3(a) and 3(b). The central frequencies of the odd modes are at $f_o^A = 193.622$ THz and $f_o^C = 193.171$ THz, while those of the even modes are at $f_e^A = 199.792$ THz and $f_e^C = 199.529$ THz, for the amorphous and crystalline states, respectively. The results can be verified by eigenfrequencies simulated by COMSOL, with values of $193.617 + 0.0018381\mathrm{i}$ THz (A) and $193.160 + 0.0255846\mathrm{i}$ THz (C) for the odd modes, while $199.708 + 0.0011476\mathrm{i}$ THz (A) and $199.453 + 0.0132981\mathrm{i}$ THz (C) for the even modes. These results are highly consistent with each other. The evolution of the eigenfrequencies is investigated in Fig. 3(c), revealing a gradual reduction with the increase of β. Besides, observations from Fig. 3(d) indicate that the Q factors of the two modes are both ultra-high ($> 10^3$). The Q factors gradually decrease with the increase of $|\beta|$, and when β tends to zero, the Q factors approach positive infinity ($+\infty$), which are both the evidence to demonstrate the symmetry-protected property of such two BICs. Notably, the Q factors of even modes are higher than those of odd modes, and the two amorphous modes exhibit higher Q factors than the crystalline modes, owing to a lower β (approaching zero). Therefore, the magnitude of the Q factor is governed directly by the material asymmetry, and inversely proportional to the value of $|\beta|$.

From the above discussion, dual quasi-BIC modes with separated eigenfrequencies are achieved in the proposed metasurface. The Q factor and GH shift can be modulated by changing the phase transition of Sb_2Se_3. However, according to Eq. (3), the phase change at the frequency of peak must be acknowledged to calculate GH shift. The corresponding characteristics of the two peaks (f_o and f_e) in two states are shown in Fig. 4. Here we convert to wavelengths to measure the GH shifts, i.e., $(\lambda_e^A, \lambda_o^A, \lambda_e^C, \lambda_o^C) = (1500.512, 1548.328, 1502.487, 1551.941)$ nm. As depicted in Figs. 4(a) and 4(b), the first row shows the reflection spectra of the amorphous state within the range of $\theta \in [2.8^\circ, 3.2^\circ]$ which both exhibit an asymmetric Fano line type. The second row reveals that the phase change at λ_e^A exhibits two slopes near 3° with the same signs but different values, yet the other of λ_o^A displays two slopes with opposite signs and values. Consequently, giant GH shifts are calculated and visualized as two negative GH shifts ($-6778\lambda_e^A$ and $-10953\lambda_e^A$) or one positive ($4174\lambda_o^A$) and one negative ($-1937\lambda_o^A$) GH shift in the bottom pictures. However, the reflection spectra in Figs. 4(c) and 4(d) feature a symmetric Lorentzian shape, and the phase change around 3° possesses merely one slope leading to similar Lorentz line-type GH shifts. Only one negative ($-697\lambda_e^C$) or one positive ($334\lambda_o^C$) GH shift is observed in the crystalline state. Therefore, when the incident angle is fixed, the GH shift of the Sb_2Se_3-based metasurface can be modulated by the incident wavelength with different directions and values. The corresponding comparison among various methods to enhance GH shifts with quasi-BICs is displayed in Table S2 of supplementary materials.

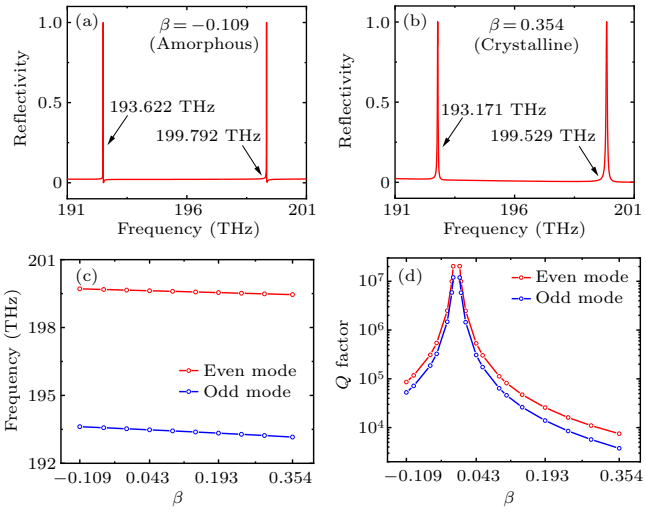


Fig. 3. Reflection spectra at the oblique incidence of $\theta = 3^\circ$, in (a) amorphous state ($\beta = -0.109$), and (b) crystalline state ($\beta = 0.354$), within $f \in [191, 201]$ THz. (c) Real part of the eigenfrequencies, and (d) the corresponding Q factors, of the even/odd modes within the range of $\beta \in [-0.109, 0.354]$.

Based on these findings, the GH shift can be feasibly obtained by the continuous modulation of the phase transition of Sb_2Se_3, which is achieved in practice by applying curated pulse voltage magnitudes and durations to the nano-heater.[31] The resultant material characteristic manifests as a variation of CR. Additionally, the CR is linked to the permittivity of Sb_2Se_3 (ε_{g1}), which in turn is influenced by β. Consequently, the relationship between CR and β can be determined by the following equation:

$$\frac{(1+\beta)\varepsilon_{g2}-1}{(1+\beta)\varepsilon_{g2}+2} = CR \times \frac{\varepsilon_{g1}^A - 1}{\varepsilon_{g1}^A + 2} + (1-CR) \times \frac{\varepsilon_{g1}^C - 1}{\varepsilon_{g1}^C + 2}. \quad (4)$$

Owing to the continuous phase transition in Sb_2Se_3, we further investigate the GH shifts of the Sb_2Se_3-based structure with other different β in addition to the previously discussed amorphous and crystalline states (see Fig. S3 of supplementary materials). All the results indicate that the incident angle for maximum GH shifts remains around 3°, while the corresponding wavelengths exhibit tiny redshifts as β increases. Considering

the Q factors of the two modes are ultrahigh for all the conditions, though such a tiny shift is only 2 nm–3 nm, it may result in large errors and potentially go undetected. Additionally, it is inconvenient to modulate the incident wavelength for exploring GH shifts since the nano-heater is always determined to be a laser (with a fixed wavelength). Therefore, the wavelength of the incident TE wave should be fixed to reveal the evolution of GH shift at different *CR*s near 3°. Here, within the range of $\theta \in [2.6°, 3.4°]$, *CR* is selected as 0%, 25%, 50%, 75%, and 100% (corresponding to $\beta = -0.109$, 0.022, 0.081, 0.204, and 0.354) at $\lambda_f = 1550$ nm for the odd mode. The GH shifts and phases of different *CR*s are presented in Figs. 5(a) and 5(b), respectively. When *CR* = 0%, the phase change is relatively smooth, and the negative slope results in a positive GH shift of approximately $322\lambda_f$. However, if *CR* changes to 25%, 50%, or 100%, the phase change demonstrates a sharp peak with two opposite slopes, leading to two opposite GH shifts. Particularly, the corresponding Q factor is highest for the case when $CR = 25\%$ ($\beta = 0.022$) compared to other cases, which is caused by the value closest to zero. The maximum GH shift can achieve around $-17368\lambda_f$ at an incident angle of 3.142° for the negative one and $20302\lambda_f$ at 3.143° for the positive one (refer to Fig. 5(b)), which shows an ultra-high sensitivity with the incident angle. When *CR* changes to 75%, there exist two negative slopes with different values, which results in two large positive GH shifts ($\sim 1000\lambda_f$) at two separated angles (2.768° and 2.907°). Notably, identical positive shifts ($\sim 200\lambda_f$) are observed at 2.75° with two *CR*s of 0% and 75%. Based on these findings, it can be concluded that once the structural parameter and incident wavelength are fixed, the Sb_2Se_3-based metasurface can exhibit giant GH shifts at different incident angles with tunable positive or negative properties due to the varying *CR*.

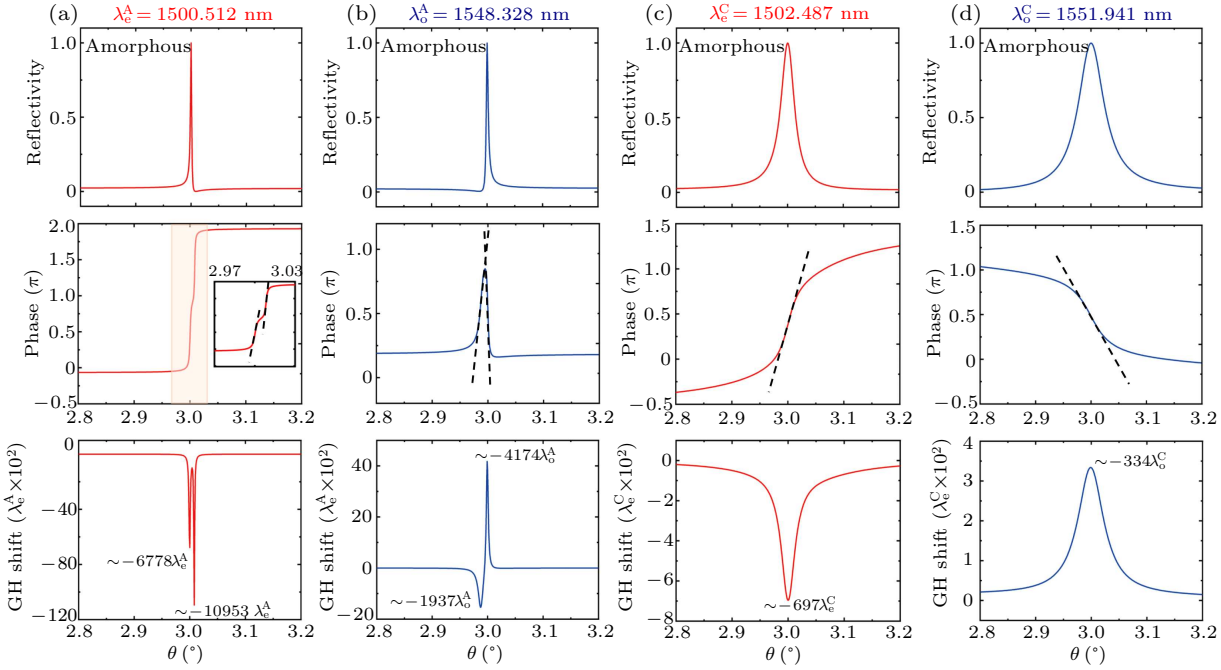


Fig. 4. Illustration of (a) the even mode ($\lambda_e^A = 1500.512$ nm) and (b) odd mode ($\lambda_o^A = 1548.328$ nm), when Sb_2Se_3 is in amorphous state. Schematic diagram of (c) the even mode ($\lambda_e^C = 1502.487$ nm) and (d) odd mode ($\lambda_o^C = 1551.941$ nm), when Sb_2Se_3 is in crystalline state. The first, second, and third rows represent the reflectivity, phase change, and GH shift, respectively. The black dashed lines are the corresponding slopes of the phase change.

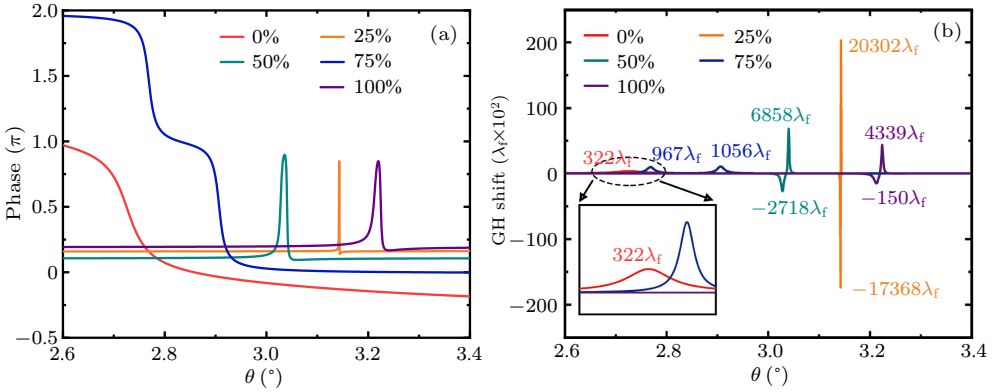


Fig. 5. (a) Phases and (b) GH shifts of the odd mode, when $CR = 0\%$, 25%, 50%, 75%, and 100% within the range of $\theta \in [2.6°, 3.4°]$. The inset represents the amplification of the case of $\theta \in [2.65°, 2.80°]$.

4. Conclusion

In conclusion, an all-dielectric Sb_2Se_3-based metasurface is proposed to obtain tunable GH shifts by introducing material asymmetry β, which is achieved through dual quasi-BIC modes generated by changing the permittivity of Sb_2Se_3 at oblique incidence. The corresponding structural parameters can be acquired by solving the dispersion relationship of the generated mode and GMR condition when the arbitrary operating wavelength and materials are determined. From above, giant-tunable GH shifts are realized in the compound structure owing to dramatic reflective phase changes. Furthermore, the values of GH shifts are proportional to the Q factors of corresponding quasi-BIC modes and inversely proportional to $|\beta|$. With its remarkable tunability, the giant bidirectional GH shifts can be achieved at various wavelengths under a fixed incident angle, or at different incident angles while upholding an operating wavelength. These novel characteristics provide a new degree of freedom, i.e., the material asymmetry β (related to the *CR* of PCMs), to realize dual quasi-BICs with bidirectional GH shifts in passive nanostructures. By employing the technologies of electron-beam lithography, the proposed metasurface could be easily fabricated,[32,34] and we expect the findings of this study can enable more capabilities in ultrasensitive sensors, optical switches, light storage, and other applications.

Acknowledgements

Project supported by the National Natural Science Foundation of China (Grant No. 12274225), the Fundamental Research Funds for the Central Universities (Grant No. NS2023056), the Natural Science Foundation of Hebei Province, China (Grant No. B2024209014), and the Basic Scientific Research Project of Hebei Provincial Department of Education (Grant No. JJC2024059).

References

[1] Goos F and Hänchen H 1947 *Annalen der Physik* **436** 333
[2] Tamir T and Oliner A A 1963 *Proc. IEEE* **51** 317
[3] Wang X, Yin C, Sun J, Li H, Wang Y, Ran M and Cao Z 2013 *Opt. Express* **21** 13380
[4] Wang X, Sang M, Yuan W, Nie Y and Luo H 2015 *IEEE Photon. Technol. Lett.* **28** 264
[5] Sattari H, Ebadollahi-Bakhtevar S and Sahrai M 2016 *J. Appl. Phys* **120** 133102
[6] Tsakmakidis K L, Boardman A D and Hess O 2007 *Nature* **450** 397
[7] Yang R, Zhu W and Li J 2015 *Opt. Express* **23** 6326
[8] Huang T Y and Yen T J 2019 *Sci. Rep.* **9** 3538
[9] Lai H and Chan S 2002 *Opt. Lett.* **27** 680
[10] Huang Y, Dong W, Gao L and Qiu C 2011 *Opt. Express* **19** 1310
[11] Kaiser R, Levy Y, Fleming J, Muniz S and Bagnato V S 1996 *Pure and Applied Optics: Journal of the European Optical Society Part A* **5** 891
[12] Zheng Z, Zhu Y, Duan J, Qin M, Wu F and Xiao S 2021 *Opt. Express* **29** 29541
[13] Chen J J, Grzegorczyk T M, Wu B I and Kong J A 2005 *J. Appl. Phys.* **98** 094905
[14] Wang Z, Wang C and Zhang Z 2008 *Opt. Commun.* **281** 3019
[15] Pan T, Xu G, Zang T and Gao L 2009 *Physica Status Solidi (b)* **246** 1088
[16] Wan Y, Zheng Z, Kong W, Zhao X, Liu Y, Bian Y and Liu J 2012 *Opt. Express* **20** 8998
[17] Li J S, Wu J F and Zhang L 2014 *IEEE Photon. J.* **6** 1
[18] Chen Y, Ban Y, Zhu Q B and Chen X 2016 *Opt. Lett.* **41** 4468
[19] Farmani A, Miri M and Sheikhi M H 2017 *Opt. Commun.* **391** 68
[20] Xue T, Li Y B, Song H Y, Wang X G, Zhang Q, Fu S F, Zhou S and Wang X Z 2023 *Chin. Phys. B* **33** 014207
[21] Xu Y, Chan C T and Chen H 2015 *Sci. Rep.* **5** 8681
[22] Wen J, Zhang J, Wang L G and Zhu S Y 2017 *JOSA B* **34** 2310
[23] Wu F, Wu J, Guo Z, Jiang H, Sun Y, Li Y, Ren J and Chen H 2019 *Phys. Rev. Appl.* **12** 014028
[24] Wu F, Luo M, Wu J, Fan C, Qi X, Jian Y, Liu D, Xiao S, Chen G, Jiang H, *et al.* 2021 *Phys. Rev. A* **104** 023518
[25] Zhang J, Ruan Y, Hu Z D, Wu J and Wang J 2023 *IEEE Sensors Journal* **23** 2070
[26] Ruan Y, Hu Z D, Wang J, Yu L and Wang Y 2022 *IEEE Photon. J.* **14** 1
[27] Cong L and Singh R 2019 *Adv. Opt. Mater.* **7** 1900383
[28] Shi W, Gu J, Zhang X, Xu Q, Han J, Yang Q, Cong L and Zhang W 2022 *Photon. Res.* **10** 810
[29] Liao Z, Ma Q, Wang L, Yang Z, Li M, Deng F and Hong W 2022 *Opt. Express* **30** 24676
[30] Jiang X, Fang B and Zhan C 2024 *Chin. Phys. B* **33** 034206
[31] Liu J, Chen C, Li X, Li J, Dong D, Liu Y and Fu Y 2023 *Opt. Express* **31** 4347
[32] Delaney M, Zeimpekis I, Lawson D, Hewak D W and Muskens O L 2020 *Adv. Func. Mater.* **30** 2002447
[33] Chen L, Hao Y, Zhao L, Wu R, Liu Y, Wei Z, Xu N, Li Z and Liu H 2021 *Opt. Express* **29** 9332
[34] Hu H, Lu W, Antonov A, Berté R, Maier S A and Tittl A 2024 *Nat. Commun.* **15** 7050